# Cyclophilin A catalyzes proline isomerization by an electrostatic handle mechanism

Carlo Camilloni[a], Aleksandr B. Sahakyan[a], Michael J. Holliday[b], Nancy G. Isern[c], Fengli Zhang[d], Elan Z. Eisenmesser[b], and Michele Vendruscolo[a,1]

[a]Department of Chemistry, University of Cambridge, Cambridge CB2 1EW, United Kingdom; [b]Department of Biochemistry and Molecular Genetics, University of Colorado, Aurora, CO 80045; [c]William R. Wiley Environmental Molecular Sciences Laboratory, High Field NMR Facility, Richland, WA 99532; and [d]National High Magnetic Field Laboratory, Tallahassee, FL 32310

Edited by Arieh Warshel, University of Southern California, Los Angeles, CA, and approved June 3, 2014 (received for review March 5, 2014)

**Proline isomerization is a ubiquitous process that plays a key role in the folding of proteins and in the regulation of their functions. Different families of enzymes, known as "peptidyl-prolyl isomerases" (PPIases), catalyze this reaction, which involves the interconversion between the *cis* and *trans* isomers of the N-terminal amide bond of the amino acid proline. However, complete descriptions of the mechanisms by which these enzymes function have remained elusive. We show here that cyclophilin A, one of the most common PPIases, provides a catalytic environment that acts on the substrate through an electrostatic handle mechanism. In this mechanism, the electrostatic field in the catalytic site turns the electric dipole associated with the carbonyl group of the amino acid preceding the proline in the substrate, thus causing the rotation of the peptide bond between the two residues. We identified this mechanism using a combination of NMR measurements, molecular dynamics simulations, and density functional theory calculations to simultaneously determine the *cis*-bound and *trans*-bound conformations of cyclophilin A and its substrate as the enzymatic reaction takes place. We anticipate that this approach will be helpful in elucidating whether the electrostatic handle mechanism that we describe here is common to other PPIases and, more generally, in characterizing other enzymatic processes.**

enzyme catalysis | NMR spectroscopy

Different families of enzymes, often referred to as "peptidyl-prolyl isomerases" (PPIases), catalyze proline isomerization, a process that involves the interconversion between the *cis* and *trans* isomers of the N-terminal amide bond of the amino acid proline (1–3). This isomerization process is an intrinsically slow reaction, typically occurring on the time scale of several minutes under physiological conditions. Hence it often represents a rate-limiting step in biochemical reactions and indeed is used ubiquitously as a molecular switch in regulation (1–7).

The possible mechanisms by which PPIases speed up this reaction have been the subject of intense scrutiny (8–16), although consensus descriptions of such mechanisms have not yet emerged. A question of particular relevance is the specific manner in which the electrostatic field in the catalytic site may facilitate the isomerization reaction. To investigate this problem, we considered the case of cyclophilin A, a member of the cyclophilin family of PPIases (17–20). Previous studies have suggested that conformations resembling those typical of the *cis*-bound and the *trans*-bound states are populated through conformational fluctuations in the free state of the enzyme and therefore functional insights into its mechanism of action might be obtained from the study of the free state (21–23).

The approach that we followed in studying the mechanism of action of cyclophilin A is based on the simultaneous determination of the structures of the *cis*-bound and *trans*-bound states of the complex between the enzyme and its substrate as the catalytic process takes place. Our results reveal that the mechanism of the reaction involves the presence of an electrostatic field that acts on the N-terminal peptide bond of the proline residue in the substrate and induces the rotation of the electric dipole corresponding to the carbonyl group of the residue preceding the proline. In this sense, the carbonyl group represents a handle operated by an electrostatic field and helps overcome the isomerization barrier.

We investigated the conformational properties of cyclophilin A during the proline isomerization process by using NMR spectroscopy, which can provide atomic-resolution descriptions of the motions of macromolecules in solution (24–32). In our strategy, NMR data are used as replica-averaged structural restraints in molecular dynamics simulations. Such calculations, which in general can include NOE-derived distances (29), $S^2$-order parameters (29), residual dipolar couplings (33–35), and chemical shifts (36–38), are particularly suitable when multiple conformations of a protein are present simultaneously in solution, because these conformations can be determined at the same time (29, 37).

## Results and Discussion

**Simultaneous Determination of the *cis*-Bound and *trans*-Bound States.** To study the proline isomerization process catalyzed by cyclophilin A, we considered the model peptide substrate GSFGPDLRAGD (39, 40). We carried out chemical shift measurements in the bound state during the catalytic reaction (*SI Text*). In addition, we used NOESY measurements to obtain information about interproton distances (i.e., intermolecular NOE restraints) between the enzyme and the substrate; therefore NOEs were measured as averages over the *cis*-bound and the *trans*-bound conformations during the isomerization reaction (*SI Text*). We then performed molecular dynamics simulations

### Significance

One of the most widespread molecular switches in biochemical pathways is based on the isomerization of the amino acid proline, a process that normally is facilitated by enzymes known as "proline isomerases." We show that cyclophilin A, one of the most common proline isomerases, acts by a simple mechanism, which we describe as an "electrostatic handle." In this mechanism, the enzyme creates an electrostatic environment in its catalytic site that rotates a peptide bond in the substrate by pulling the electric dipole associated with the carbonyl group preceding the peptide bond itself. Our results thus identify a specific mechanism by which electrostatics is exploited in enzyme catalysis.

Author contributions: C.C., A.B.S., E.Z.E., and M.V. designed research; C.C., A.B.S., M.J.H., E.Z.E., and M.V. performed research; C.C., N.G.I., F.Z., E.Z.E., and M.V. contributed new reagents/analytic tools; C.C., A.B.S., M.J.H., E.Z.E., and M.V. analyzed data; and C.C., M.J.H., E.Z.E., and M.V. wrote the paper.

The authors declare no conflict of interest.

This article is a PNAS Direct Submission.

[1]To whom correspondence should be addressed. Email: mv245@cam.ac.uk.

This article contains supporting information online at www.pnas.org/lookup/suppl/doi:10.1073/pnas.1404220111/-/DCSupplemental.

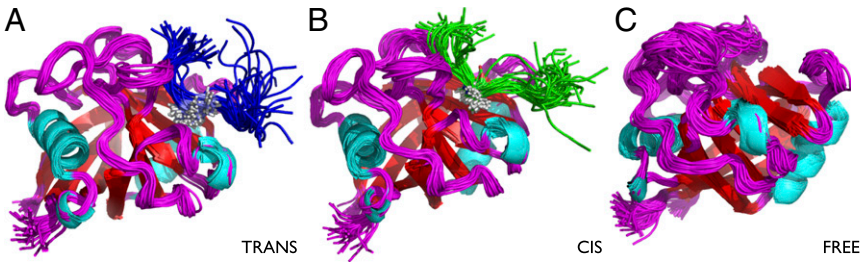


**Fig. 1.** Ensembles of structures representing the conformational fluctuations of cyclophilin A in the *trans*-bound (*A*), the *cis*-bound (*B*), and the free (*C*) states. The ensembles have been determined using backbone chemical shifts as replica-averaged restraints (free state) and backbone chemical shifts and interchain NOEs replica-averaged restraints (bound state). The simulations were performed with a modified version of GROMACS, using the Amber99SB*-ILDN force-field and applying the CamShift and NOE restraints over two replicas (37). More details are provided in *SI Text*.

with replica-averaged chemical shifts (37) and intermolecular NOE restraints (29), a technique that enables the information provided by NMR measurements to be incorporated in the structural determination procedure in a manner consistent with the maximum entropy principle (41–43). We used two replicas of the system; the initial structures were chosen with the proline in the model peptide in the *cis* conformation in the first replica and in the *trans* conformation in the second replica (*SI Text*). These calculations resulted in two (*cis*-bound and *trans*-bound) conformational ensembles (Fig. 1) with corresponding free-energy landscapes (Fig. 2). The agreement between experimental and calculated intermolecular NOEs and chemical shifts was excellent (Table S1 and Fig. 3). For comparison, we also carried out similar calculations for the free state of the enzyme (Fig. 2; see also *Conformational Fluctuations in the Free State*).

**A Possible Electrostatic Handle Mechanism of Catalysis.** To formulate a hypothesis about the mechanism of catalysis, we analyzed the ensemble of conformations representing the bound state of cyclophilin A and its substrate. This ensemble can be divided into *cis*-bound and *trans*-bound subensembles. We then considered the overall electrostatic field in the active site of the enzyme (44), prompted by the observation that the presence of a conserved arginine residue at position 55 (R55) is known to play a key role in the function of cyclophilin A (13–15). More specifically, density functional theory (DFT) calculations (*SI Text*) of the electrostatic field acting on the glycine–proline peptide bond were carried out for the *cis*-bound and the *trans*-bound ensembles (Figs. S1–S3). Our results indicate that the *z* component, defined as the normal to the ring plane defined by the N, Cα, and Cγ atoms of the proline residue, is approximately the same for the *cis*-bound and the *trans*-bound states (Fig. 4).

Having determined the electrostatic field present in the active site of cyclophilin A during the catalytic process, we investigated its specific effect on the proline isomerization process. To obtain an initial insight into this effect, we performed DFT calculations (*SI Text*) on a model system, the *N*-acetyl-L-prolyl-*N*-methyl-amide (Ace-Pro-Nme) proline dipeptide, in vacuo and compared the potential energy surface of this system in the presence and absence of an electrostatic field corresponding to that found in the active site of cyclophilin A. The potential energy surfaces for the isomerization process as a function of the ω and ψ angles (Fig. 4) indicate that in the absence of electrostatic fields the *trans* isomer is about 20 kJ/mol more stable than the *cis* isomer, with the clockwise (ω = −90°) and counterclockwise (ω = 90°) energy barriers between the *cis*-bound and *trans*-bound states being of comparable height ("clockwise" and "counterclockwise" are defined for the *trans*-to-*cis* transition) (Fig. 4).

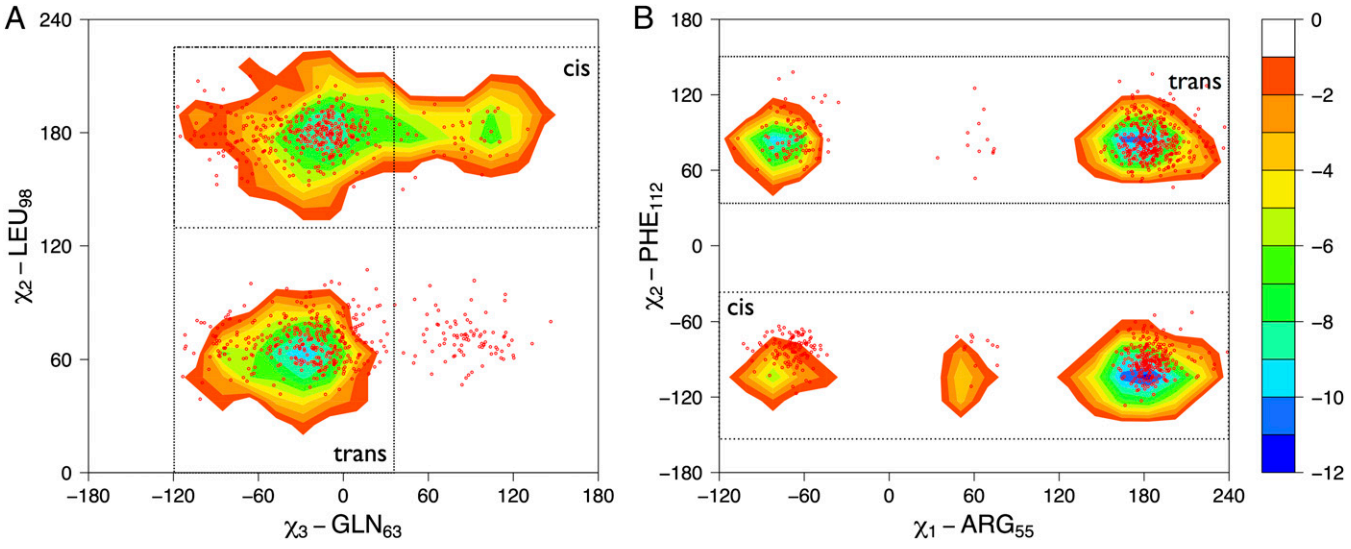


**Fig. 2.** Cyclophilin A samples regions of its conformational space in the absence of the substrate similar to those sampled during the catalytic turnover. Free-energy surfaces for the bound state of cyclophilin A as a function of active site and protein core side chains are shown. (*A*) Free-energy landscape as a function of the $\chi_3$ dihedral angle of GLN63 and the $\chi_2$ dihedral angle of LEU98. (*B*) Free-energy landscape as a function of the $\chi_1$ dihedral angle of ARG55 and the $\chi_2$ dihedral angle of PHE112. The isolines are plotted at intervals of 2.0 kJ/mol. The contours represent the *trans*-bound– and *cis*-bound–specific basins; the red dots represent the free ensemble.

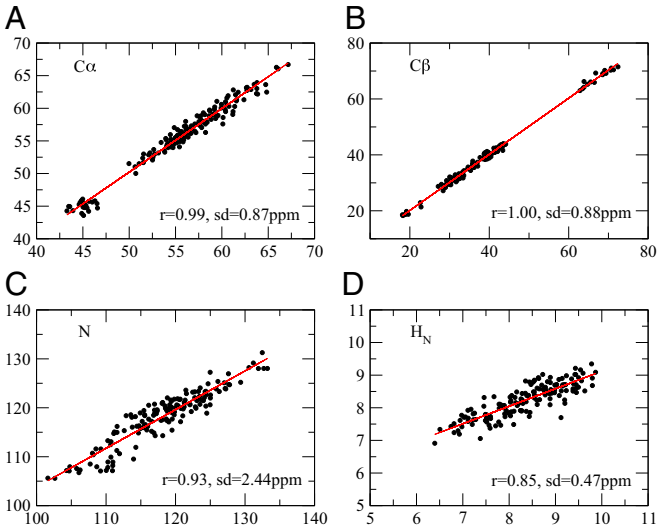


**Fig. 3.** Comparison between the experimental and calculated chemical shifts for the bound-state ensemble of cyclophilin A. (*A*) Cα atoms, (*B*) Cβ atoms, (*C*) N atoms, and (*D*) HN atoms. *r*, correlation coefficient; *sd*, SE.

The potential energy surface of the proline dipeptide model in the presence of an electrostatic field of 50 MV/cm along the negative direction of the *z* axis is shown in Fig. 4. In this case the main effect of the electrostatic field is to reduce the energy barrier strongly, by about 30 kJ/mol, at ω = 90° while slightly increasing the energy barrier at ω = −90°. Furthermore this electrostatic field increases the stability of the *cis*-bound state by about 10 kJ/mol. Previous studies that used classic molecular dynamics simulations suggested that cyclophilin A catalyzes proline isomerization along a counterclockwise direction for the *trans*-to-*cis* transition (14, 15).

Here, our model calculations enable us to put forward the hypothesis that, perhaps not surprisingly, the source of this effect is the electrostatic field generated by the enzyme in its catalytic site and acting on the glycine–proline peptide bond. These results, more in detail, also suggest that the effect of cyclophilin A is to create an electrostatic handle that acts on the electric dipole of the glycine carbonyl group of the glycine–proline substrate (Movie S1), which is the only substantial electric dipole in proximity of the glycine–proline peptide bond, thus stabilizing the transition state in which the dipole is aligned with the field (ω = 90). The lowering of the barrier (i.e., the stabilization of the transition state) is compatible with the experimentally observed speed-up of four to five orders of magnitude (from minutes to milliseconds) of the isomerization process.

To investigate the presence of possible additional effects of the electrostatic field on the electron density in correspondence to the peptide bond, we performed a natural bond orbital analysis (*SI Text*) that clearly indicated that the electron density along

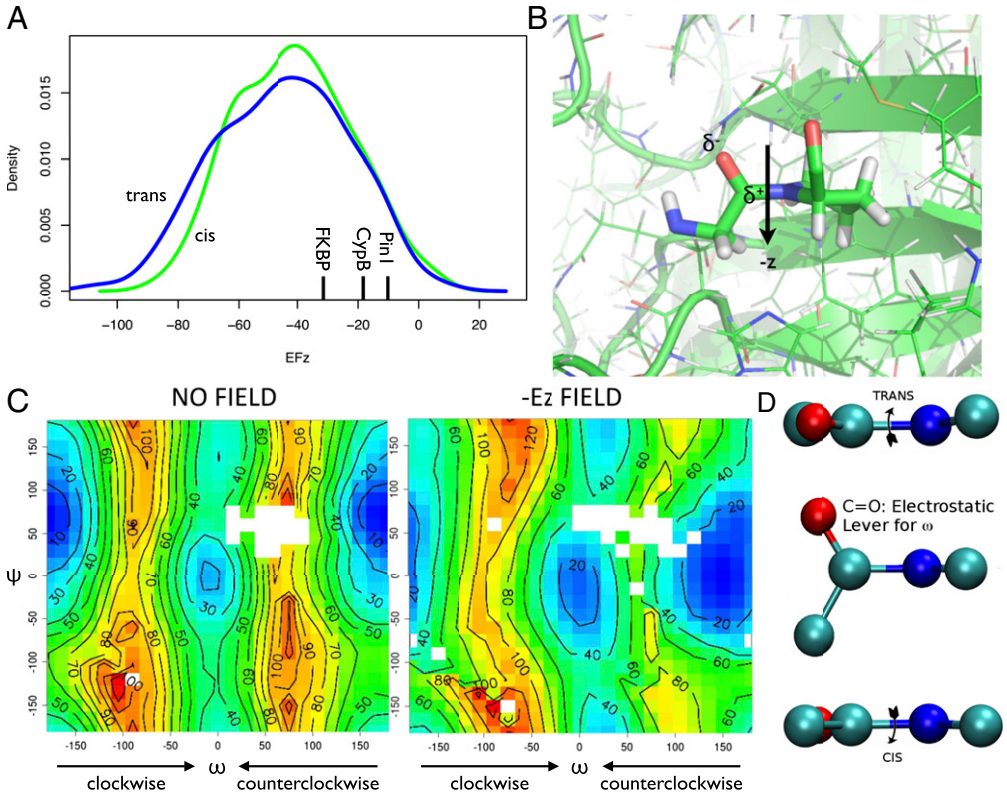


**Fig. 4.** (*A*) Probability distributions of the electrostatic field (in megavolts per centimeter) components along the *z* axis. The *cis*-bound ensemble is shown in green and the *trans*-bound ensemble in blue. The electrostatic field was calculated from the electronic density derived by DFT (*SI Text*). (*B*) Illustration of the electrostatic handle mechanism (see also Movie S1). (*C*) Potential energy surfaces (in kilojoules per mole) of the Ace-Pro-Nme peptide in vacuo with and without an electric field of the magnitude found in the active site of cyclophilin A. The potential energy surfaces were calculated at the same level of accuracy (*SI Text*) as the electric field of *A*. The negative value of the *z* component of the field, which has same magnitude in both the *cis*-bound and the *trans*-bound states, has the effect of reducing the potential energy barrier between the *cis* (ω = 0) and *trans* (ω = 180°) in the positive direction (from 0° to 180°), whereas it increases the barrier in the negative direction (from 0° to −180°). (*D*) Schematic illustration of the electrostatic handle mechanism of proline isomerization. The electric field in the catalytic site acts on the electric dipole associated with the carbonyl group of the glycine preceding the proline in the substrate, thus causing a rotation in the ω angle of the peptide bond between the two residues.

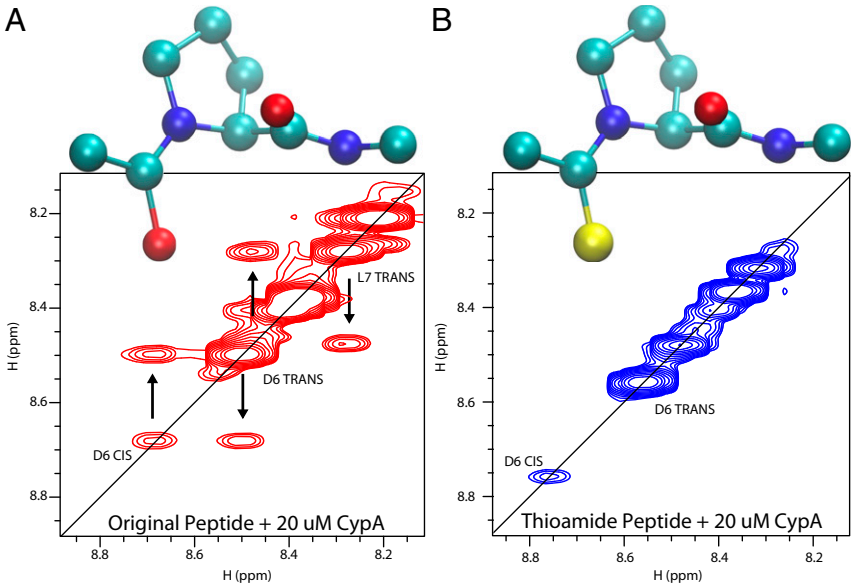


**Fig. 5.** Homonuclear NOESY spectra of the model peptide (*A*) and thioamide-substituted peptide (*B*) in the presence of 20 μM cyclophilin A after a 200-ms mixing time. Exchange peaks, which indicate isomerization, are visible for the model peptide but not for the thioamide-substituted peptide. The sulfur atom is shown in yellow in *B*.

the peptide bond is almost completely unaffected by the presence of the electrostatic field, showing that the nature of the chemical bond remains unchanged.

**Validation of the Electrostatic Handle Mechanism with a Thioamide-Substituted Peptide.** To test the electrostatic handle mechanism suggested by the model calculations described above, we selectively altered the electrostatic properties of the handle by replacing the CO group with a CS group in the glycine residue preceding the proline in the substrate. The replacement of an oxygen atom by a sulfur atom modifies the substrate primarily by reducing the electrostatic dipole of the handle (i.e., the CO group in the wild-type peptide and the CS group in the modified peptide) and thus is expected to reduce the catalytic activity of cyclophilin A. Indeed, a calculation of the electrostatic potential charge on the Ace-Pro-Nme proline dipeptide in vacuo indicates that replacing a CO group by a CS group reduces the value of the dipole from 0.65 eÅ for the CO bond to 0.35 eÅ for the CS bond. Assuming that the average electrostatic field in the active site of cyclophilin A is 40 MV/cm, one can estimate the increase in the isomerization barrier associated with the CS replacement to be ∼10 kJ/mol, corresponding to a slowing down of the isomerization process by approximately two orders of magnitude.

We verified that the thioamide modification alters the binding affinity only marginally (Fig. S4), but, consistently with the above prediction, the absence of exchange peaks in the homonuclear NOESY spectrum (Fig. 5) and the absence of cross-peaks in the ZZ-exchange spectrum (Fig. S5) correspond to a lack of proline isomerization in the thioamide-substituted peptide.

**Further Support for the Electrostatic Handle Mechanism from the R55A Mutant.** To characterize better the specific contribution to the total electrostatic field of the arginine residue at position 55 (R55), which has been proposed to be key in the catalytic process (22, 23), the DFT calculations were repeated over the same ensemble of bound structures but with an R55A mutation. The analysis of the electric field distributions in this case is consistent with the observation of an almost complete loss of enzymatic activity of this mutation (22). Indeed, the $z$ component of the electrostatic field is strongly reduced (Fig. 6). In the R55A variant, the electrostatic field lowers the isomerization barrier by less than 15 kJ/mol, to about half the value in the wild-type R55. These calculations confirmed that R55 plays a key role in the catalysis by generating the electrostatic field that turns the carbonyl group of glycine and by keeping the proline in place by a hydrogen bond with its side chain. Overall, the global effect of the electrostatic field is to reduce the counterclockwise barrier, thus making the isomerization process much more accessible, as well as stabilizing the alternative isomerization state.

**Other PPIases.** To investigate whether the electrostatic handle mechanism is specific for cyclophilin A or is used more generally by other PPIases, we calculated the electrostatic field acting on the carbonyl group in three other structures representing the three major families of PPIases: immunophilins (including cyclophilins), FK506-binding proteins (FKBPs), and parvulins (3). Our results were consistent with those found for cyclophilin A: −19 MV/cm for cyclophilin B (PDB ID code 1VAI), −33 MV/cm for an FKBP (PDB ID code 4ITZ), and −10 MV/cm for Pin1 (PDB ID code 1PIN), a parvulin (Fig. 4*A*). These values of the electrostatic field indicate, but do not prove, that the electrostatic handle mechanism may be common among PPIases, although other effects also may contribute to the isomerization process in different cases (1–3).

The values of the electrostatic field shown in Fig. 4*A* for individual structures also illustrate the importance of determining an ensemble of conformations representing the dynamics of the enzyme because individual structures may exhibit low values of the electrostatic field just by chance, thus making it difficult to identify the importance of the electrostatic field in the catalytic mechanism.

**Conformational Fluctuations in the Free State.** We then applied the approach we used for the bound states, i.e., using molecular dynamics simulations with chemical shift restraints (but this time without NOE restraints), to characterize the free conformations of cyclophilin A (Fig. 1*C*). In this case also, the agreement between experimental and calculated chemical shifts was excellent (Fig. S6). Moreover, in the absence of the substrate, residual dipolar couplings (RDCs) were readily obtained for cyclophilin

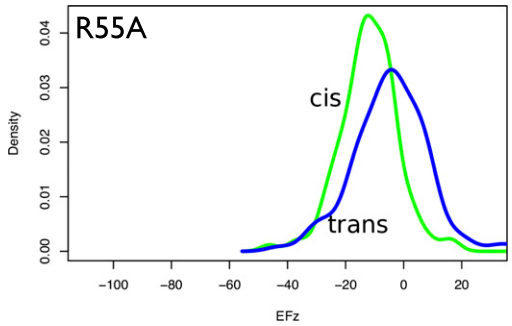


**Fig. 6.** Comparison between the probability distributions of the electrostatic field component (in megavolts per centimeter) along the *z* axis for the R55A mutant in the *cis*-bound and *trans*-bound states. The corresponding distributions for wild-type R55 (Fig. 4*A*) are shifted to the left by about 30 MV/cm.

A (*SI Text*). The free-state ensemble thus was validated by using RDC data, which were not used in the structure calculations (Fig. S7). We found that the Q factor for the X-ray structure of PDB ID code 1OCA (45) is 0.45, whereas that of the ensemble is 0.31.

From relaxation-dispersion measurements of the free (21, 22, 39) and bound (46) states of cyclophilin A, it has been suggested that the conformational fluctuations of these states are similar (21–23). Recently presented crystal structures of the free state (23) showed that two populations could be characterized in terms of different rotameric states of a specific set of amino acids. An analysis of the ensembles determined in this work demonstrates that in the free state of cyclophilin A the *cis*-bound–like and the *trans*-bound–like conformations are in conformational exchange (i.e., these functionally relevant conformations already are being sampled in the absence of the substrate). These results are illustrated by plotting the free-energy surface for the free state of cyclophilin A as a function of the rotameric state of four amino acids belonging either to the active site or to the core of the protein. The *cis*-bound and *trans*-bound ensembles are clearly included in the free-energy surface of the free enzyme (Fig. 2). Further analysis of the conformational fluctuations of the side chains shows that, in particular for S99 and F113, the free ensemble that we determined is fully consistent with previous results (23) (Fig. S8). The coexistence of *cis*-bound–like and *trans*-bound–like conformations in the free state of cyclophilin A is a defining trait of the high conformational mobility of this enzyme in the absence of a substrate.

**Concluding Remarks.** To characterize the mechanism by which cyclophilin A catalyzes proline isomerization, we simultaneously determined the *cis*-bound and *trans*-bound states of the enzyme as the catalytic reaction takes place (Fig. 1). This result was obtained by using NMR spectroscopy in combination with molecular dynamics simulations. In our approach, the NMR measurements are used as replica-averaged structural restraints in molecular dynamics simulations (29, 37, 41–43). Because the experimental information is used to restrain the average values corresponding to the measured quantities over multiple copies of the protein molecules, it is possible to take into account the conformational flexibility of the molecules themselves (Figs. 1 and 2).

By analyzing the electrostatic field in the catalytic site in the ensembles of conformations that we determined, which represent the *cis*-bound and *trans*-bound states of the peptide substrate in complex with cyclophilin A, we identified an electrostatic handle mechanism underlying the catalytic process (Fig. 4 and Movie S1). We then validated this mechanism by studying the proline isomerization process of a modified version of the substrate, in which we performed a targeted change in the electric dipole representing the handle. We obtained this result by replacing the oxygen atom of the carbonyl group of the amino acid preceding the proline with a sulfur atom, a specific substitution that concerns a single atom in the substrate and conserves the group in the periodic table. As expected, this rationally designed substitution, which significantly reduces the electric dipole of the handle but leaves the other properties of the substrate essentially unchanged, suppressed significantly the catalytic activity of cyclophilin A (Fig. 5).

These results also provide further insights into the possible roles of dynamics in catalysis (21–23, 27, 47–50) when no chemical bond is formed or broken, because the conformational fluctuations in the bound state, which resemble those previously described in the free state (21–23), enable the population of structures that are particularly effective in reducing the isomerization barrier by providing the appropriate electrostatic fields (Fig. 4*A*).

More generally, our findings illustrate that the combination of NMR spectroscopy with molecular dynamics simulations and quantum mechanical calculations has the potential of identifying the specific mechanisms by which enzymes use electrostatic fields for catalysis.

## Methods

Expression and purification of recombinant $^{13}C$,$^{15}N$-labeled cyclophilin A were carried out as described in *SI Text*. The measurements of chemical shifts and residual dipolar couplings in the free and peptide-bound states (including the bound state with the thioamide-substituted peptide) were carried out as described in *SI Text*. Molecular dynamics simulations with replica-averaged NMR restraints and quantum mechanical calculations were carried out as described in *SI Text*.

**ACKNOWLEDGMENTS.** We are grateful to Dr. Francesco Aprile for useful discussions. Part of this research was performed using the facilities of the Environmental Molecular Sciences Laboratory, a national scientific user facility sponsored by the Office of Biological and Environmental Research of the Department of Energy located at Pacific Northwest National Laboratory, Richland, WA. C.C. was supported by a Marie Curie Intra European Fellowship.

1. Fischer G, Bang H, Mech C (1984) Detection of enzyme catalysis for cis-trans-isomerization of peptide-bonds using proline-containing peptides as substrates. *Biomed Biochim Acta* 43:1101–1111.
2. Göthel SF, Marahiel MA (1999) Peptidyl-prolyl cis-trans isomerases, a superfamily of ubiquitous folding catalysts. *Cell Mol Life Sci* 55(3):423–436.
3. Lu KP, Finn G, Lee TH, Nicholson LK (2007) Prolyl cis-trans isomerization as a molecular timer. *Nat Chem Biol* 3(10):619–629.
4. Andreotti AH (2003) Native state proline isomerization: An intrinsic molecular switch. *Biochemistry* 42(32):9515–9524.
5. Eakin CM, Berman AJ, Miranker AD (2006) A native to amyloidogenic transition regulated by a backbone trigger. *Nat Struct Mol Biol* 13(3):202–208.
6. Eckert B, Martin A, Balbach J, Schmid FX (2005) Prolyl isomerization as a molecular timer in phage infection. *Nat Struct Mol Biol* 12(7):619–623.
7. Sarkar P, Saleh T, Tzeng SR, Birge RB, Kalodimos CG (2011) Structural basis for regulation of the Crk signaling protein by a proline switch. *Nat Chem Biol* 7(1):51–57.
8. Fanghänel J, Fischer G (2004) Insights into the catalytic mechanism of peptidyl prolyl cis/trans isomerases. *Front Biosci* 9:3453–3478.
9. Fischer S, Michnick S, Karplus M (1993) A mechanism for rotamase catalysis by the FK506 binding protein (FKBP). *Biochemistry* 32(50):13830–13837.
10. Jakob RP, Schmid FX (2009) Molecular determinants of a native-state prolyl isomerization. *J Mol Biol* 387(4):1017–1031.
11. Sarkar P, Reichman C, Saleh T, Birge RB, Kalodimos CG (2007) Proline cis-trans isomerization controls autoinhibition of a signaling protein. *Mol Cell* 25(3):413–426.
12. Trzesniak D, van Gunsteren WF (2006) Catalytic mechanism of cyclophilin as observed in molecular dynamics simulations: Pathway prediction and reconciliation of X-ray crystallographic and NMR solution data. *Protein Sci* 15(11):2544–2551.
13. Zydowsky LD, et al. (1992) Active site mutants of human cyclophilin A separate peptidyl-prolyl isomerase activity from cyclosporin A binding and calcineurin inhibition. *Protein Sci* 1(9):1092–1099.
14. Hamelberg D, McCammon JA (2009) Mechanistic insight into the role of transition-state stabilization in cyclophilin A. *J Am Chem Soc* 131(1):147–152.

15. Leone V, Lattanzi G, Molteni C, Carloni P (2009) Mechanism of action of cyclophilin A explored by metadynamics simulations. *PLoS Comput Biol* 5(3):e1000309.
16. Li G, Cui Q (2003) What is so special about Arg 55 in the catalysis of cyclophilin A? insights from hybrid QM/MM simulations. *J Am Chem Soc* 125(49):15028–15038.
17. Handschumacher RE, Harding MW, Rice J, Drugge RJ, Speicher DW (1984) Cyclophilin: A specific cytosolic binding protein for cyclosporin A. *Science* 226(4674):544–547.
18. Fischer G, Wittmann-Liebold B, Lang K, Kiefhaber T, Schmid FX (1989) Cyclophilin and peptidyl-prolyl cis-trans isomerase are probably identical proteins. *Nature* 337(6206): 476–478.
19. Wang P, Heitman J (2005) The cyclophilins. *Genome Biol* 6(7):226.
20. Davis TL, et al. (2010) Structural and biochemical characterization of the human cyclophilin family of peptidyl-prolyl isomerases. *PLoS Biol* 8(7):e1000439.
21. Eisenmesser EZ, Bosco DA, Akke M, Kern D (2002) Enzyme dynamics during catalysis. *Science* 295(5559):1520–1523.
22. Eisenmesser EZ, et al. (2005) Intrinsic dynamics of an enzyme underlies catalysis. *Nature* 438(7064):117–121.
23. Fraser JS, et al. (2009) Hidden alternative structures of proline isomerase essential for catalysis. *Nature* 462(7273):669–673.
24. Wüthrich K (1989) Protein structure determination in solution by nuclear magnetic resonance spectroscopy. *Science* 243(4887):45–50.
25. Bax A (2003) Weak alignment offers new NMR opportunities to study protein structure and dynamics. *Protein Sci* 12(1):1–16.
26. Mittermaier A, Kay LE (2006) New tools provide new insights in NMR studies of protein dynamics. *Science* 312(5771):224–228.
27. Boehr DD, Dyson HJ, Wright PE (2006) An NMR perspective on enzyme dynamics. *Chem Rev* 106(8):3055–3079.
28. Kalodimos CG (2011) NMR reveals novel mechanisms of protein activity regulation. *Protein Sci* 20(5):773–782.
29. Lindorff-Larsen K, Best RB, Depristo MA, Dobson CM, Vendruscolo M (2005) Simultaneous determination of protein structure and dynamics. *Nature* 433(7022):128–132.
30. Markwick PRL, et al. (2010) Enhanced conformational space sampling improves the prediction of chemical shifts in proteins. *J Am Chem Soc* 132(4):1220–1221.
31. Robustelli P, Stafford KA, Palmer AG, 3rd (2012) Interpreting protein structural dynamics from NMR chemical shifts. *J Am Chem Soc* 134(14):6365–6374.
32. Shaw DE, et al. (2010) Atomic-level characterization of the structural dynamics of proteins. *Science* 330(6002):341–346.
33. Clore GM, Schwieters CD (2004) How much backbone motion in ubiquitin is required to account for dipolar coupling data measured in multiple alignment media as assessed by independent cross-validation? *J Am Chem Soc* 126(9):2923–2938.
34. Lange OF, et al. (2008) Recognition dynamics up to microseconds revealed from an RDC-derived ubiquitin ensemble in solution. *Science* 320(5882):1471–1475.
35. Montalvao RW, De Simone A, Vendruscolo M (2012) Determination of structural fluctuations of proteins from structure-based calculations of residual dipolar couplings. *J Biomol NMR* 53(4):281–292.
36. Robustelli P, Kohlhoff K, Cavalli A, Vendruscolo M (2010) Using NMR chemical shifts as structural restraints in molecular dynamics simulations of proteins. *Structure* 18(8): 923–933.
37. Camilloni C, Robustelli P, De Simone A, Cavalli A, Vendruscolo M (2012) Characterization of the conformational equilibrium between the two major substates of RNase A using NMR chemical shifts. *J Am Chem Soc* 134(9):3968–3971.
38. Neudecker P, et al. (2012) Structure of an intermediate state in protein folding and aggregation. *Science* 336(6079):362–366.
39. Schlegel J, et al. (2009) Solution characterization of the extracellular region of CD147 and its interaction with its enzyme ligand cyclophilin A. *J Mol Biol* 391(3):518–535.
40. Bahmed K, et al. (2012) Extracellular cyclophilin-A stimulates ERK1/2 phosphorylation in a cell-dependent manner but broadly stimulates nuclear factor kappa B. *Cancer Cell Int* 12(1):19.
41. Cavalli A, Camilloni C, Vendruscolo M (2013) Molecular dynamics simulations with replica-averaged structural restraints generate structural ensembles according to the maximum entropy principle. *J Chem Phys* 138(9):094112.
42. Pitera JW, Chodera JD (2012) On the use of experimental observations to bias simulated ensembles. *J Chem Theory Comput* 8:3445–3451.
43. Roux B, Weare J (2013) On the statistical equivalence of restrained-ensemble simulations with the maximum entropy method. *J Chem Phys* 138(8):084107.
44. Warshel A, et al. (2006) Electrostatic basis for enzyme catalysis. *Chem Rev* 106(8): 3210–3235.
45. Ottiger M, Zerbe O, Güntert P, Wüthrich K (1997) The NMR solution conformation of unligated human cyclophilin A. *J Mol Biol* 272(1):64–81.
46. Bosco DA, et al. (2010) Dissecting the microscopic steps of the cyclophilin A enzymatic cycle on the biological HIV-1 capsid substrate by NMR. *J Mol Biol* 403(5):723–738.
47. Kamerlin SCL, Warshel A (2010) At the dawn of the 21st century: Is dynamics the missing link for understanding enzyme catalysis? *Proteins* 78(6):1339–1375.
48. Glowacki DR, Harvey JN, Mulholland AJ (2012) Taking Ockham's razor to enzyme dynamics and catalysis. *Nat Chem* 4(3):169–176.
49. Schwartz SD, Schramm VL (2009) Enzymatic transition states and dynamic motion in barrier crossing. *Nat Chem Biol* 5(8):551–558.
50. Nashine VC, Hammes-Schiffer S, Benkovic SJ (2010) Coupled motions in enzyme catalysis. *Curr Opin Chem Biol* 14(5):644–651.

# Supporting Information

## Camilloni et al. 10.1073/pnas.1404220111

### SI Text

**NMR Measurements.** ***Chemical shifts in the free state.*** Recombinant $^{13}C$,$^{15}N$-labeled cyclophilin A was purified as described previously (1). Briefly, $^{13}C$,$^{15}N$-labeled cyclophilin A was concentrated to ∼1.0 mM protein in 50 mM $Na_2HPO_4$ (pH 6.5), 2 mM DTT with 10% $D_2O$, which was the NMR solution buffer. All spectra were collected on either a Varian 600 MHz or 800 MHz spectrometer at 10 °C and at 25 °C, which included a standard Biopack HNCACB and CBCAcoNH. Data were processed using NMRPipe (2) and analyzed using CcpNmr software (3).

***Chemical shifts and intermolecular NOEs in the bound state.*** To obtain NMR measurements in the bound state of cyclophilin A with the GSFGPDLRAGD peptide substrate, two samples were produced. The first sample contained 0.5 mM $^{13}C$,$^{15}N$-labeled cyclophilin A and 4 mM of unlabeled peptide, and the second sample contained 0.5 mM $^{13}C$,$^{15}N$-labeled peptide with 4 mM of unlabeled cyclophilin A. This two-sample strategy was used because of the relatively weak binding constant between cyclophilin A and the peptide substrate, which makes it impossible to approach saturation for both the enzyme and the peptide. Instead, a 1:8 ratio allows ∼97% binding, such that the chemical shifts report on the bound form. This strategy also reduces peak overlap. The buffer described above for the free enzyme was used. Because the *cis*-to-*trans* and *trans*-to-*cis* substrate isomerization rates are 1,040/s and 1,640/s, respectively (4), catalysis is within the fast exchange regime. Thus, chemical shifts during catalysis obtained for each of the two samples described above provide values averaged over the *cis*-bound and *trans*-bound states. At these concentrations the enzyme and peptide are about 97% bound. C13/N15-edited/filtered intermolecular NOESY experiments, Biopack sequence gCNfilnoesyChsqcSA, were collected using these two samples, and the resulting NOEs were used for the calculations.

***Residual dipolar couplings in the free state.*** Commercially available bicelle mixtures were found to interact specifically with the hydrophobic active site of cyclophilin A as monitored through $^{15}N$-heteronuclear single-quantum coherence (HSQC) spectroscopy experiments. As previously described, specific mixtures offer optimal alignment at different temperatures. Thus, C12E5/hexanol mixtures were produced for amide residual dipolar couplings (RDCs) collected at 25 °C, whereas C8E5/octanol mixtures were produced for amide RDCs collected at both 10 °C and 0 °C. For example, 30 μL of polyethylene glycol was added to the NMR solution buffer, and alcohols were added at microliter increments; during these additions the monodeuterated water splitting was used to monitor alignment of these mixtures. Finally, 60 μL of 1.1 mM $^{15}N$-labeled cyclophilin A was added to 240 μL of the aligned mixtures, and standard in-phase/anti-phase experiments were collected on a Varian 900 MHz at the Rocky Mountain Regional 900 MHz NMR Facility at the three temperatures described above.

**Molecular Dynamics Simulations.** ***General setup.*** All the simulations in the present work were performed using GROMACS (5). The system was simulated using the Amber99SB*-ILDN force field (6, 7) in explicit TIP3P water (8). A time step of 2 fs was used together with LINCS constraints (9). van der Waals interactions were cut off at 1.2 nm, and long-range electrostatic interactions were treated with the Particle Mesh Ewald method (10). The canonical ensemble was enforced by keeping the volume fixed and by thermosetting the system with the Bussi thermostat (11). The starting conformation for the free state was taken from the NMR structure of Protein Data Bank (PDB) ID code 1OCA (12); the structures of PDB ID codes 1M9C and 1M9Y were used for the *cis*-bound and *trans*-bound states, respectively (13). The structures were protonated and solvated with 5,102 TIP3P water molecules in a dodecahedron box with a volume of 178 $nm^3$. First, the energy of the system was minimized, and then the temperature was increased to 300 K in two separate steps. In the first step a 50-ps simulation was performed by keeping the heavy atoms of the protein fixed; then a second 200-ps simulation was performed without any restraint. The density of the system was relaxed by a 200-ps run using the Berendsen barostat (14).

***Replica-averaged ensemble.*** The starting structures for the two replicas of the system were selected as the final structure from two simulations, each 1 ns long. Experimental chemical shifts for the free and bound state were measured as described in the *NMR* section above and were applied as a restraint over the two replicas of the system as shown previously for ribonuclease A (15). CamShift (16) was used to back-calculate the chemical shifts from both replicas at each time step. In the bound case, the NOEs between the protein and the substrate were applied on the two replicas as average restraints (17, 18).

The force constant for the chemical shifts restraints was set to 5.2 kJ/mol, and the force constant for the NOEs was set to 250 $kJ{\cdot}mol^{-1}{\cdot}nm^{-2}$ with a bottom flat potential that is zero between 0.3 and 0.5 nm. In term of energy per atom, the contribution of the chemical shifts restraint was less than 0.4 kJ/mol (<3% of the total), and the contribution of the NOEs was less than 0.02 kJ/mol (<1% of the total). Each replica has been evolved through a series of annealing cycles between 300 K and 450 K (100 ps at 300 K, 100 ps during which the temperature increased linearly up to 450 K, 100 ps of constant-temperature molecular dynamics at 450 K, and 300 ps during which the temperature decreased linearly to 300 K). Only structures from the 300-K segment of the simulation are taken into account for analysis. Each replica has been evolved for a total nominal time of 100 ns. The final ensembles comprise all the 300-K structures sampled by both replicas.

The averaged chemical shift restraints were added to GROMACS by using PLUMED (19) and Almost. The NOEs were added using the module already provided within GROMACS.

**Quantum Mechanical Calculations.** All the quantum mechanical (QM) calculations were done using the Gaussian 03 suite of programs (20).

***Investigation of electric field effects on the ω–ψ potential energy surface of a proline model.*** The starting calculations aimed to reveal the presence of electrostatic field effects on the energy barrier of ω rotation at the substrate proline site. A bicapped L-proline was used as a model to study the influence of electrostatic fields (Fig. S4). The acetylic (*Ace*) and *N*-methyl amino (*Nme*) groups were added at the L-proline imino and carboxyl termini, respectively. The resulting structure (*N*-acetyl-L-prolyl-*N*-methylamide, Ace-Pro-Nme) is the simplest model for studying the properties of a proline residue while maintaining relatively correct electronic states of the terminal atoms that, in a full-scale polypeptide structure, participate in peptide bonding with the adjacent amino acid residues.

Hybrid-density functional theory (DFT) (21) was used with the Becke three-parameter exchange functional and the Lee, Yang, and Parr correlation functional (22–24) (B3LYP) for all QM calculations in this work.

The geometry of the model was constructed manually using mixed Cartesian and internal coordinates to maintain a fixed direction for the molecule-associated coordinate system over the course of conformational changes in the molecule but retaining the ability to relax the structure fully when a complete geometry optimization was needed. The origin of the coordinate system is set at the N atom of proline, with the *x* axis always pointing along the N–C bond and the *z* axis orthogonal to the plane of the proline ring as represented in Fig. S2*B*. The choice of the axis directions also accounted for the predicted most influential directions for the uniform electric fields. The *y* direction is along the (H)–N bond and is parallel to the C=O bonds of the peptide bond that defines the ω rotation, with (H) being a carbon atom in the case of proline imino acid. The *z* axis points in the direction of the formation of a nonconventional hydrogen-bond between the proline nitrogen and the guanidinium moiety of arginine or histidine from an enzyme-binding site. This hydrogen bond represents a widely accepted mechanism for the action of the proline isomerization enzymes (25). In many cases hydrogen bonding can be regarded as a type of electric field effect (26); hence the further generalization of the H-bonding as electric field effects seems to be a reasonable explanation for the actions of cyclophilins. Overall, the *x* and *z* directions selected for the further application of a uniform electric field should be most influential in changing the energetic characteristics of the ω rotation.

The initial structure of Ace-Pro-Nme was fully geometry optimized with a split-valence 6–31G(d,p) basis set (27). This step was followed by a complete scan of the ψ and ω space, spanning the range of −180° to 180° for both angles with angle steps of 15°. For each ψ/ω configuration, the geometry was optimized with preset ψ and ω angles in nine different conditions, overall completing 5,625 (25 × 25 × 9) hybrid-DFT calculations. The nine conditions include eight calculations with uniform electric fields of −50, −20, 0, 20, and 50 MV/cm (the minus signs indicate the reverse direction) applied along the *x* and *z* directions and a single calculation without any external field application. The complete set of results is presented in Fig. S4, where the energy of the Ace-Pro-Nme system is plotted against the ω and ψ angles under the above conditions. The energy is presented in kilojoules per mole, referenced by the lowest energy conformation observed in each of the computed landscapes. The difference map between the corresponding electric field condition and the normal, gas-phase (no field) condition clearly highlights the regions in the ψ/ω space where the electric field stabilizes (blue) or destabilizes (red) the system (Fig. S4).

As can be inferred from the potential energy surface plots, the electric field acting along both the *x* and *z* directions has a substantial impact on the pathway of the ω-rotation reaction. It is clear that the electric fields along the *–x, x, –z*, and *z* directions facilitate ω rotations by decreasing the relative barrier for the transitions at the 0/+, +/(−,+), 0/+ and +/− regions correspondingly. In *a*/*b* notation, *a* indicates the region of the ψ dihedral angle (around 0, + for positive ψ, and − for negative ψ), and *b* denotes the same for ω (Fig. S4). Hence, the fine interplay of electrostatic fields acting along different directions is capable of modulating the pathway for the proline *cis–trans* transitions.

***Natural bond orbital analysis of Ace-Pro-Nme.*** To clarify whether the effect of the electric field on the ω-rotation barrier is the result of substantial changes in the electronic structure at the proline site, we performed a natural bond orbital (NBO) (28, 29) analysis of Ace-Pro-Nme, paying attention to the bonding orbital along the N–C bond that defines the ω rotation. In particular, if the influence of the external electric field were mediated through abrupt changes in electronic structure, one would expect a decrease in the population of the N–C bonding orbital components and/or a decrease in the contributions from the natural atomic orbitals in *p* components and increase in these contributions in *s* components. With such changes, the N–C bond can become more of an *s* type and less of a *p* type, thus making the rotation along the bond relatively more feasible.

However, the results show only slight differences in such populations upon the application of the electric field. For instance, the selected model transition structure with ω = 90° and ψ = −10°, for which a substantial reduction of the potential energy is observed while applying −50-MV/cm field along the *z* axis (Fig. S4*B*), changes the N–C binding natural molecular orbital from [0.7903($sp^{2.39}$) + 0.6128($sp^{2.22}$)] to [0.7911($sp^{2.45}$) + 0.6117($sp^{2.29}$)], as expressed in the established notation system for the NBO analysis and omitting negligible *d* contributions. The first term in the addition comes from N atoms, and the second term from C atoms. The polarization coefficients, if squared, show the percentage of the NBO on each N-based or C-based hybrid. Shown below is the state of the N–C bonding NBO with and without a −50 MV/cm uniform electric field, with the whole system expressed in percentages and the *sp* hybrids broken down into separate *s* and *p* contributions:

Electrostatic field = 0 MV/cm

NBO occupancy = 1.98605

Orbital energy = −0.75419 Hartree

N (62.45% contribution, of which 29.45% is *s* character and 70.50% is *p* character)

C (37.55% contribution, of which 31.02% is *s* character and 68.84% is *p* character)

Electrostatic field = − 50 MV/cm along the *z* axis

NBO occupancy = 1.98519

Orbital energy = −0.74989 Hartree

N (62.58% contribution, of which 28.97% is *s* character and 70.97% is p character)

C (37.42% contribution, of which 30.34% is *s* character and 69.52% is *p* character)

Hence, the electrostatic field affected the overall electron occupancy of the N–C bonding NBO only slightly, increasing (slightly destabilizing) the orbital energy by ∼11.3 kJ/mol and slightly increasing the *p* character of the contributing natural atomic orbitals. Similar negligible effects are observed in similar calculations using the *cis* (ω = 0° and ψ = −10°) and *trans* (ω = 180° and ψ = −10°) structures of the proline model instead of the transition-state structure.

Therefore, the observed stabilization of the transition structure is the result of the overall electrostatic interaction of the substrate molecule with the external electric fields rather than specific modulation of the electronic structure that would affect the N–C bond of the ω rotation.

***QM studies of the electric fields in the active site of cyclophilin A.*** The calculations for the proline residue model detailed above clearly demonstrate that electric fields with values within the range typical for biomolecules (30) can be influential in defining ω-rotation energy barriers. Here we also verify that the fields of such magnitude are acting in cyclophilin A active site.

For the QM calculations on the cyclophilin A active site, 114 structures from each of the obtained *cis* and *trans* ensembles were geometry optimized with an Amber99SB*-ILDN force field (6, 7). The maximum allowed force acting on any atom was set at 100 kJ/nm. An active region is defined for cyclophilin A via an *n*-layered integrated molecular orbital plus molecular mechanics method (ONIOM) (31) routine in Gaussian 03. The region is determined first by counting all the atoms within a 7.5-Å radius from the nitrogen atom of the substrate proline. Next, the fragments from the residues that were halved by this definition were extended to complete the residues or, in the case of large

residues, to extend the moieties toward a chemically sensible partition. The latter step has set the distance of the most distant (from proline N) counted atoms at around 12 Å. The resulting QM region included 250 atoms from Arg-55, Ile-57, Phe-60, Met-61, Gln-63, Met-100, Ala-101, Asn-102, Ala-103, Phe-113, Trp-121, Leu-122, Lys-125, and His-126 (Fig. S3).

In this way, ONIOM calculations are done for all of the 228 structures from *cis* and *trans* ensembles. Single-point calculations were done with B3LYP/6–31G(d,p) level of theory for the system inside the QM region. Dummy atoms replaced the substrate atoms, so that only the electrostatic contribution from cyclophilin A was counted, and the place markers for the substrate atoms were retained. Electrostatic effect embedding was not allowed; hence the electric fields in the cyclophilin A active site reflect only the QM component from the defined region. Then, electric field values were retrieved for the position of the substrate N atom of the proline residue and then were projected into the $x$ and $z$ coordinates of the proline N-fixed coordinate system.

All the calculations described here were repeated for the equivalent set of structures from *cis* and *trans* ensembles with the R55A mutation.


1. Schlegel J, et al. (2009) Solution characterization of the extracellular region of CD147 and its interaction with its enzyme ligand cyclophilin A. *J Mol Biol* 391(3):518–535.
2. Delaglio F, et al. (1995) NMRPipe: A multidimensional spectral processing system based on UNIX pipes. *J Biomol NMR* 6(3):277–293.
3. Vranken WF, et al. (2005) The CCPN data model for NMR spectroscopy: Development of a software pipeline. *Proteins* 59(4):687–696.
4. Eisenmesser EZ, et al. (2005) Intrinsic dynamics of an enzyme underlies catalysis. *Nature* 438(7064):117–121.
5. Hess B, Kutzner C, van der Spoel D, Lindahl E (2008) Gromacs 4: Algorithms for highly efficient, load-balanced, and scalable molecular simulation. *J Chem Theory Comput* 4(3):435–447.
6. Best RB, Hummer G (2009) Optimized molecular dynamics force fields applied to the helix-coil transition of polypeptides. *J Phys Chem B* 113(26):9004–9015.
7. Lindorff-Larsen K, et al. (2010) Improved side-chain torsion potentials for the Amber ff99SB protein force field. *Proteins* 78(8):1950–1958.
8. Jorgensen WL (1981) Quantum and statistical mechanical studies of liquids. 10. Transferable intermolecular potential functions for water, alcohols, and ethers - application to liquid water. *J Am Chem Soc* 103:335–340.
9. Hess B (2008) P-lincs: A parallel linear constraint solver for molecular simulation. *J Chem Theory Comput* 4:116–122.
10. Essmann U, et al. (1995) A smooth particle mesh Ewald method. *J Chem Phys* 103: 8577–8593.
11. Bussi G, Donadio D, Parrinello M (2007) Canonical sampling through velocity rescaling. *J Chem Phys* 126(1):014101.
12. Ottiger M, Zerbe O, Güntert P, Wüthrich K (1997) The NMR solution conformation of unligated human cyclophilin A. *J Mol Biol* 272(1):64–81.
13. Howard BR, Vajdos FF, Li S, Sundquist WI, Hill CP (2003) Structural insights into the catalytic mechanism of cyclophilin A. *Nat Struct Biol* 10(6):475–481.
14. Berendsen HJC, Postma JPM, van Gunsteren WF, Dinola A, Haak JR (1984) Molecular-dynamics with coupling to an external bath. *J Chem Phys* 81:3684–3690.
15. Camilloni C, Robustelli P, De Simone A, Cavalli A, Vendruscolo M (2012) Characterization of the conformational equilibrium between the two major substates of RNase A using NMR chemical shifts. *J Am Chem Soc* 134(9):3968–3971.
16. Kohlhoff KJ, Robustelli P, Cavalli A, Salvatella X, Vendruscolo M (2009) Fast and accurate predictions of protein NMR chemical shifts from interatomic distances. *J Am Chem Soc* 131(39):13894–13895.
17. Lindorff-Larsen K, Best RB, Depristo MA, Dobson CM, Vendruscolo M (2005) Simultaneous determination of protein structure and dynamics. *Nature* 433(7022): 128–132.
18. Richter B, Gsponer J, Várnai P, Salvatella X, Vendruscolo M (2007) The MUMO (minimal under-restraining minimal over-restraining) method for the determination of native state ensembles of proteins. *J Biomol NMR* 37(2):117–135.
19. Bonomi M, et al. (2009) PLUMED: A portable plugin for free-energy calculations with molecular dynamics. *Comput Phys Commun* 180:1961–1972.
20. Frisch MJ, et al. (2004) *Gaussian 03, revision c.02* (Gaussian, Inc, Wallingford, CT).
21. Kohn W, Sham LJ (1965) Self-consistent equations including exchange and correlation effects. *Phys Rev* 140:1133–1138.
22. Lee C, Yang W, Parr RG (1988) Development of the Colle-Salvetti correlation-energy formula into a functional of the electron density. *Phys Rev B Condens Matter* 37(2): 785–789.
23. Becke AD (1993) Density-functional thermochemistry. 3. The role of exact exchange. *J Chem Phys* 98:5648–5652.
24. Miehlich B, Savin A, Stoll H, Preuss H (1989) Results obtained with the correlation-energy density functionals of Becke and Lee, Yang and Parr. *Chem Phys Lett* 157: 200–206.
25. Schroeder OE, et al. (2006) Theoretical and experimental investigation of the energetics of cis-trans proline isomerization in peptide models. *J Phys Chem A* 110(20):6522–6530.
26. Sahakyan AB, Shahkhatuni AG, Shahkhatuni AA, Panosyan HA (2008) Electric field effects on one-bond indirect spin-spin coupling constants and possible biomolecular perspectives. *J Phys Chem A* 112(16):3576–3586.
27. Krishnan R, Binkley JS, Seeger R, Pople JA (1980) Self-consistent molecular-orbital methods. 20. Basis set for correlated wave-functions. *J Chem Phys* 72:650–654.
28. Foster JP, Weinhold F (1980) Natural hybrid orbitals. *J Am Chem Soc* 102:7211–7218.
29. Reed AE, Weinhold F (1983) Natural bond orbital analysis of near-Hartree-Fock water dimer. *J Chem Phys* 78:4066–4073.
30. Suydam IT, Snow CD, Pande VS, Boxer SG (2006) Electric fields at the active site of an enzyme: Direct comparison of experiment with theory. *Science* 313(5784):200–204.
31. Vreven T, Morokuma K (2000) On the application of the IMOMO (integrated molecular orbital plus molecular orbital) method. *J Comput Chem* 21:1419–1432.
32. Fraser JS, et al. (2009) Hidden alternative structures of proline isomerase essential for catalysis. *Nature* 462(7273):669–673.

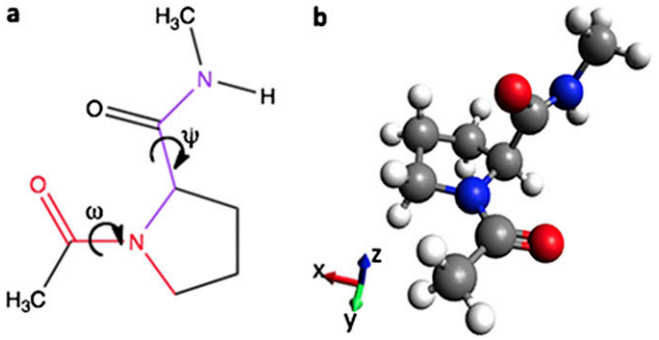


**Fig. S1.** Molecular model used to obtain the energy profiles of proline conformational transitions at different electric field values and directions. (*A*) The ω and ψ dihedral angles, further used as potential energy-surface coordinates, are highlighted. (*B*) An example of the geometry is shown with the directions of the coordinate system that is attached to the N atom of proline.

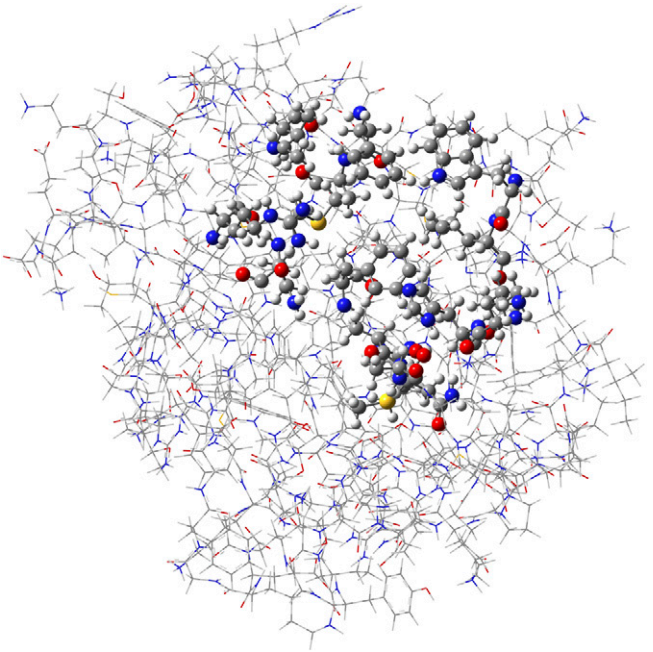

**Fig. S2.** Structure of cyclophilin A showing the QM region around the active substrate-binding site highlighted in ball-and-stick representation.

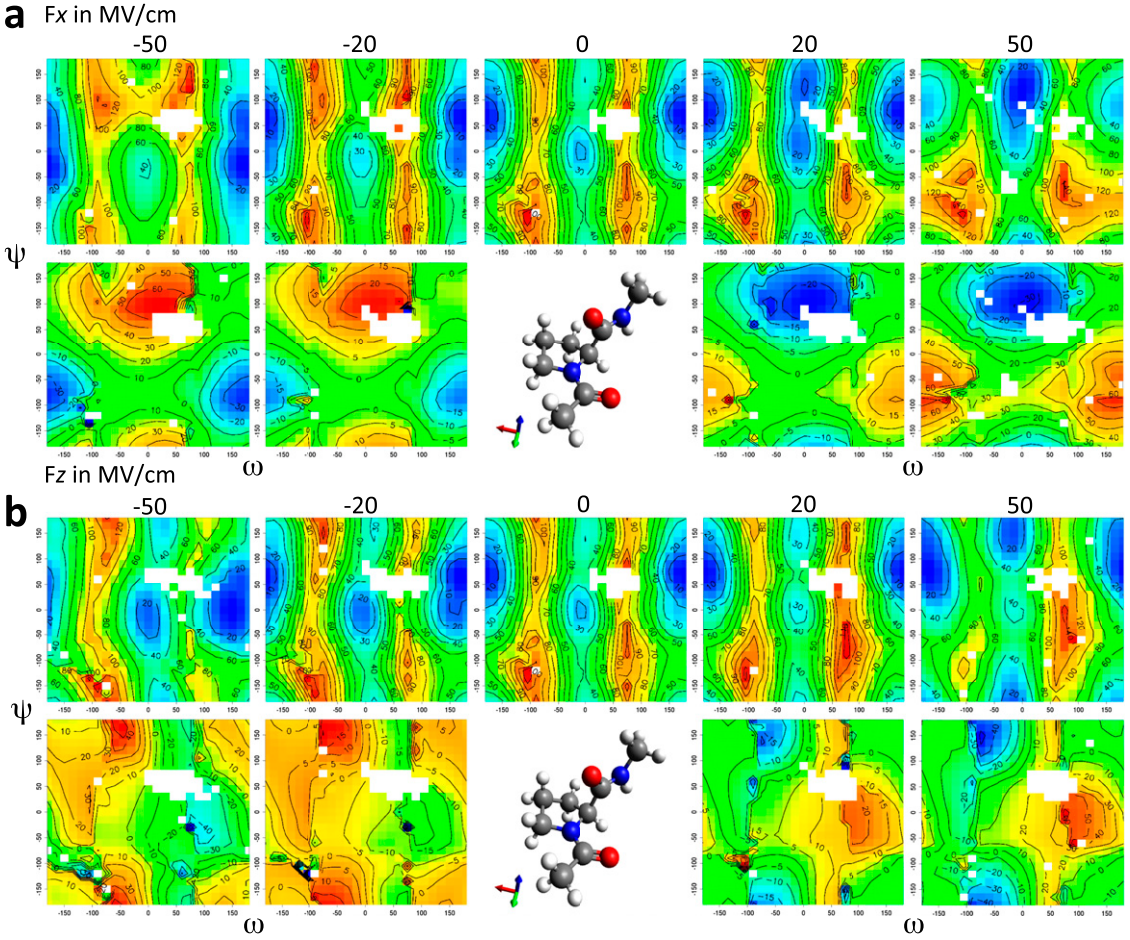


**Fig. S3.** Potential energy surfaces for Ace-Pro-Nme across ψ/ω space without and with uniform electric field acting along the *x* (*A*) and *z* (*B*) directions. The color scheme (from blue to red) and the isocontour lines depict the energy in kilojoules per mole. The lower rows in *A* and *B* show difference maps calculated with respect to the model system in the absence of an electric field.

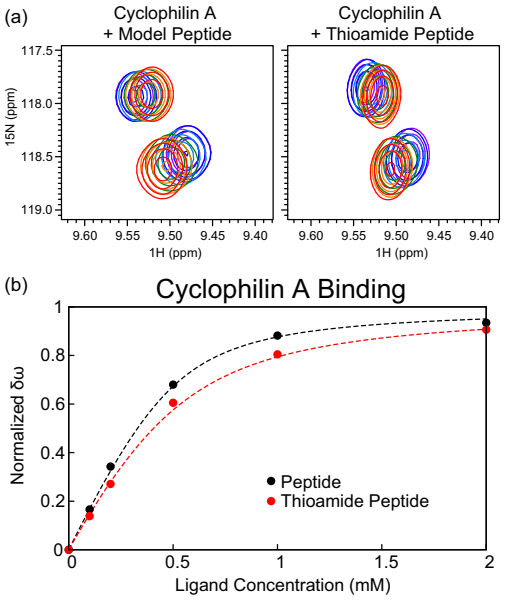


**Fig. S4.** Binding of the thioamide-substituted peptide. (*A*) HSQC spectra of 0.5 mM $^{15}$N CypA alone (red) or with addition of 0.1 mM (orange), 0.2 mM (green), 0.5 mM (light blue), 1 mM (dark blue), and 2 mM (violet) model peptide (*Left*) or thioamide-substituted peptide (*Right*). (*B*) Normalized binding isotherm for a single residue in CypA during titration of the model peptide (black) and modified peptide (red). Dotted lines represent best-fit curves using the dissociation constant determined by simultaneous fitting to multiple peaks for each titration. The dissociation constants for the model and thioamide-substituted peptide are 76 ± 6 μM and 156 ± 16 μM, respectively.

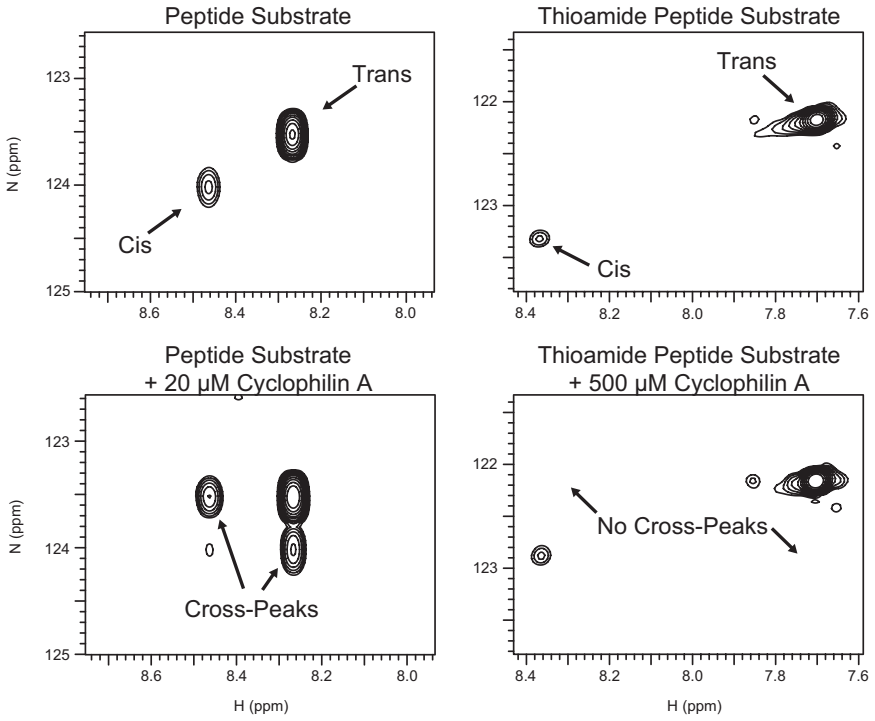


**Fig. S5.** Comparison of the ZZ-exchange spectra of the model peptide substrate and its thioamide variant. The spectra of the peptides alone and with cyclophilin A (20 μM added to the normal peptide, 500 μM added to the thioamide peptide variant) are shown. Although there are no cross-peaks in the thioamide peptide variant, even with 500 μM cyclophilin A, the *cis* peak is shifted significantly, consistent with the observation that cyclophilin A binds to the *cis* conformation. These results indicate that the thioamide substitution almost completely stops the turnover of the substrate.

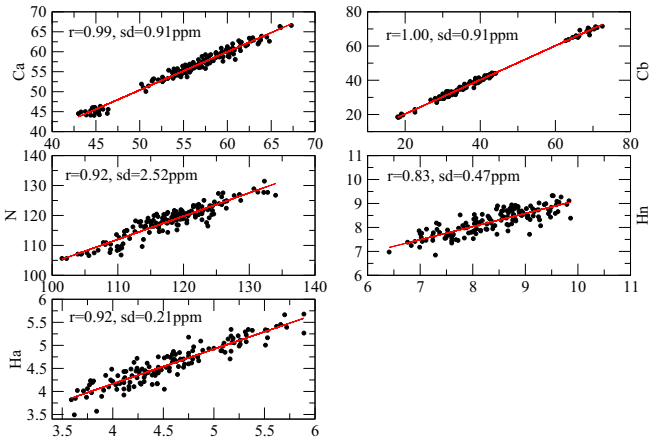


**Fig. S6.** Comparison of the experimental and calculated chemical shifts for the free-state ensemble of cyclophilin A. *r*, correlation coefficient; sd, SE.

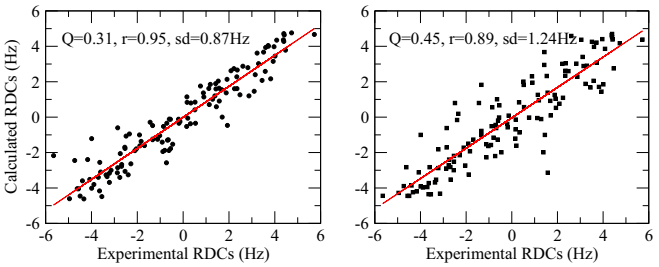


**Fig. S7.** Comparison of the experimental and calculated RDCs. (*Left*) Free ensemble of cyclophilin A. (*Right*) The structure of PDB ID 1OCA. Q, quality factor; r, correlation coefficient; sd, SE.

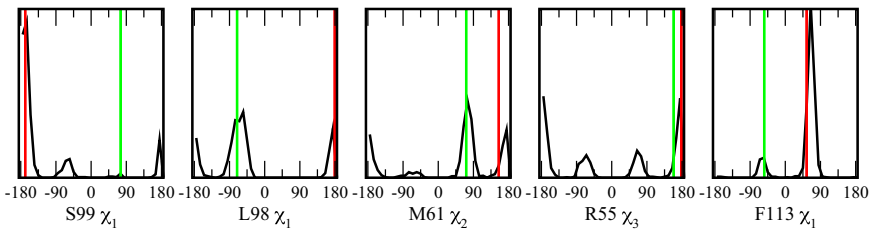


**Fig. S8.** Comparison of dihedral angles in the free conformations determined by Fraser et al. (32) and in the present study. The black line represents the free-state ensembles of cyclophilin A; the red and green bars represent the major and minor population, respectively, as determined by Fraser et al. (32).

**Table S1. Distances (in nanometers) for the hydrogen atom pairs restrained with NOE-derived distances**

| Atom pairs | *cis* subensemble | *trans* subensemble | Whole ensemble | Experimental range |
|---|---|---|---|---|
| **73Hg–1Ha** | 0.43 | 0.53 | 0.46 | 0.2–0.6 |
| 73Hg–2Ha | 0.37 | 0.31 | 0.33 | 0.2–0.6 |
| 73Hg–2Hb | 0.42 | 0.44 | 0.43 | 0.2–0.6 |
| 73Hg–3Hd | 0.51 | 0.50 | 0.51 | 0.2–0.6 |
| 73Hg–3He | 0.49 | 0.52 | 0.51 | 0.2–0.6 |
| **100He–3Hd** | 0.40 | **0.84** | 0.44 | 0.2–0.6 |
| **100He–3He** | 0.36 | **0.77** | 0.40 | 0.2–0.6 |
| **102Ha–3Hd** | 0.41 | 0.30 | 0.33 | 0.2–0.6 |
| 102Ha–3He | 0.44 | 0.35 | 0.38 | 0.2–0.6 |
| **102Hb–3Hd** | **0.67** | 0.57 | 0.60 | 0.2–0.6 |
| **102Hb–3He** | **0.70** | 0.57 | 0.61 | 0.2–0.6 |
| 107Hb–3Hd | 0.45 | 0.50 | 0.47 | 0.2–0.6 |
| 107Hb–3He | 0.30 | 0.31 | 0.30 | 0.2–0.6 |
| 107Hg–3Hd | **0.66** | **0.72** | **0.68** | 0.2–0.6 |
| 107Hg–3He | 0.55 | 0.56 | 0.55 | 0.2–0.6 |
| **108Ha–3Hd** | **0.70** | 0.56 | 0.60 | 0.2–0.6 |
| **108Ha–3He** | 0.58 | 0.42 | 0.46 | 0.2–0.6 |
| 122Hd–6Ha | 0.59 | **0.65** | 0.61 | 0.2–0.6 |
| **122Hd–6Hb** | 0.42 | **0.61** | 0.46 | 0.2–0.6 |
| **148Hg–7Hd** | **0.66** | 0.48 | 0.52 | 0.2–0.6 |
| 148Hd–7Hd | 0.60 | 0.52 | 0.55 | 0.2–0.6 |
| 57Hd–7Hd | 0.41 | 0.45 | 0.43 | 0.2–0.6 |
| 57Hg–7Hd | 0.41 | 0.36 | 0.38 | 0.2–0.6 |
| 60Ha–7Hd | 0.58 | 0.55 | 0.56 | 0.2–0.6 |
| 60Hb–7Hd | 0.40 | 0.36 | 0.23 | 0.2–0.6 |
| **61He–7Hd** | 0.53 | **0.77** | 0.59 | 0.2–0.6 |
| 119Hg–7Hd | **0.71** | **0.69** | **0.70** | 0.2–0.6 |

The columns show the averages for the *cis*-bound and *trans*-bound subensembles and for the whole bound ensemble. Values in bold are outside the experimental bounds.

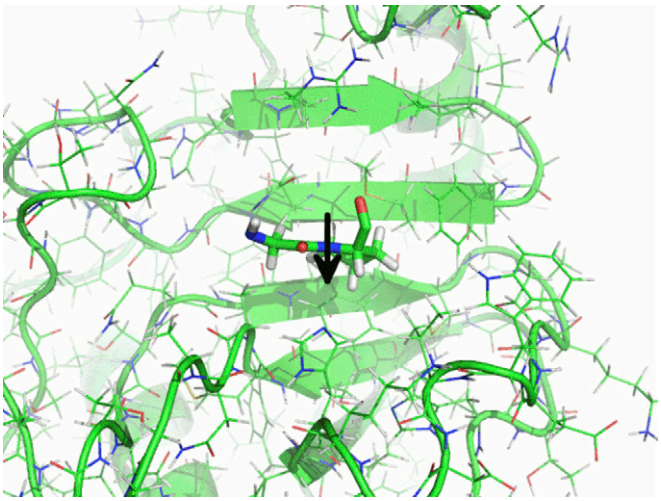

**Movie S1.** Illustration of the electrostatic handle mechanism. (*Left*) The electrostatic field (black arrow) in the catalytic site of cyclophilin A acts on the electric dipole associated with the carbonyl group of the glycine residue preceding the proline residue in the peptide substrate, thus favoring its rotation. (*Right*)The energy barrier for the rotation is shown as a function of the ω (*x*-axis) and ψ (*y*-axis) backbone dihedral angles.

Movie S1